DALTON
FULL PAPER

Alkali metal and magnesium enamides from metallation of the alkyl ligands [(2-Pyr)($SiMe_3$)CH_2] and [6-Me-(2-Pyr)($SiMe_3$)-CH_2]: a solid state and *ab initio* study†

Philip C. Andrews,*[a] David R. Armstrong,[b] Colin L. Raston,[a] Brett A. Roberts,[a] Brian W. Skelton[c] and Allan H. White[c]

[a] *Department of Chemistry, Monash University, Clayton, Melbourne, Vic. 3800, Australia*
[b] *Department of Pure and Applied Chemistry, University of Strathclyde, Glasgow, G1, Scotland UK*
[c] *Department of Chemistry, University of Western Australia, Nedlands, Perth, W.A. Australia*

Received 30th November 2000, Accepted 13th February 2001
First published as an Advance Article on the web 19th March 2001

The alkali metal complexes [**r**Na·(pmdta)]$_2$, **1**, [**r**K·(pmdta)]$_2$, **2**, [**r**Na·(tmeda)]$_2$, **3**, [**r**′Li·(pmdta)], **4**, and the magnesium complex, [(**r**)$_2$Mg·(hmpa)$_2$], **5**, formed on metallation of the monosilylated ligands [(2-Pyr)($SiMe_3$)CH_2] (= **r**H) and [6-Me-(2-Pyr)($SiMe_3$)CH_2] (= **r**′H), rather than being metal alkyls, are all metal enamides in the solid state, as evidenced by single crystal X-ray diffraction studies. Even in the presence of the bi- and tri-dentate donors tmeda (= *N*,*N*,*N*′,*N*′-tetramethylethylenediamine) and pmdta (= *N*,*N*,*N*′,*N*′,*N*″-pentamethyldiethylenetriamine) the heavier alkali metal complexes are found to be dimeric. The Li complex is monomeric and adopts the enamide configuration despite the presence of additional steric bulk on introduction of a Me group on the 6-position of the pyridyl ring. This preference for an enamide configuration, rather than that of carbanion or aza-allyl, has been studied by *ab initio* MO calculations. These confirmed that as the coordination environment of the metal increases the enamide form rather then the aza-allylic form becomes the most energetically favoured configuration.

Introduction

The organometallic chemistry of the bulky bis-silylated alkyl ligand, (2-Pyr)($SiMe_3$)$_2C^-$, **R**, has been extensively investigated.[1] This is due, in part, to the ligand having several attractive features; it is devoid of a β-H, thereby negating the possibility of low energy β-hydride elimination processes, it has the available stabilising effect of a nearby pyridyl N, and there is kinetic protection offered by the two Me_3Si groups. In contrast, the monosilylated ligand, (2-Pyr)($SiMe_3$)CH^-, **r**, is less bulky and only retains the possible stabilising effect of the pyridyl N. It is not surprising therefore, that the structural chemistry of this ligand is far less developed.[2]

Through solid state studies of their lithium complexes it is now well established that the picolyl anions can adopt three resonance forms; carbanion, enamide and η^3-aza-allyl, Fig. 1.

Complexes containing the bis-silylated ligand, [**R**Li·(L)$_k$]$_n$, have been shown to adopt the carbanion form, *e.g.* [**R**Li]$_2$, and more often the aza-allyl form, *e.g.*, [**R**Li·(**R**H)], [**R**Li·(tmeda)]. Complexes containing the monosilylated ligand, [**r**Li·(L)$_k$]$_n$, are also commonly found to adopt the aza-allyl form, *e.g.*, [**r**Li·(Et$_2$O)]$_2$, but are also found in the enamide form, *e.g.* [**r**Li·(tmeda)]$_2$, [**r**Li·(sparteine)].[2] To-date there have been no examples of complexes with **R** in the enamide form or of **r** in the carbanion form. It is interesting to note that all those p-block and transition metal complexes of **R** which have been structurally authenticated in the solid state adopt the alkyl form, with the main bond being that of M–C_{ipso}.[1,3] However, recent investigations into other substituted picolyl derivatives reveal that a greater degree of structural diversity is possible. The bis-substituted ligands, [(2-Pyr)(Ph)$_2$CM·(L)$_k$], (M = Li, L = Et$_2$O, *k* = 2; M = Na, L = thf, *k* = 3; M = K, L = pmdta/thf)[4] and [(2-Pyr)(Ph)($SiMe_3$)CLi·(tmeda)][5] all have the anion in the enamide form, as do the mono-substituted complexes, [(2-Pyr)-(Me$_2$^{t}BuSi)HCLi·(tmeda)]$_2$ and [(2-Pyr)(Ph)HCLi·(tmeda)]$_2$, which are dimeric and share the common feature of a central four membered (NLi)$_2$ planar ring.[5]

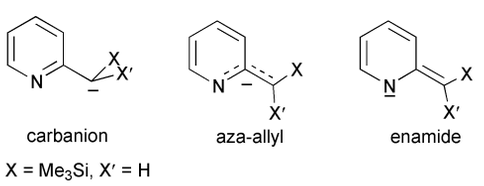

Fig. 1 Tautomeric forms of the picolyl anion.

Explanations for the various adopted geometries are based on the ability of the anion to delocalise negative charge, thus allowing the metal flexibility in achieving the most energetically stable coordination environment, the nature of the substituents on the *ipso* carbon and the role of any Lewis donors present.

It was of interest to us to expand the studies on the lithium complexes of the monosilylated ligand, **r**, to complexes of the heavier alkali metals, and to Mg, in order to obtain a more complete picture of the electronic and steric effects on the adopted structures, and also to probe in more detail the reasons for the alkyl to amide shift. In addition, we have also investigated what effect, if any, there is on preferred structural arrangement on introducing a Me group on the 6-position of the ligand, [6-Me-(2-Pyr)($SiMe_3$)HC^-], **r**′. To that end, we have synthesised and structurally characterised by single crystal X-ray crystallography the following five complexes; [**r**Na·(pmdta)]$_2$, **1**, [**r**K·(pmdta)]$_2$, **2**, [**r**Na·(tmeda)]$_2$, **3**, [**r**′Li·(pmdta)], **4**, [(**r**)$_2$Mg·(hmpa)$_2$], **5**, and have undertaken an *ab initio* study into reasons why the structural rearrangement occurs.

† The authors dedicate this paper to the memory of Ron Snaith.

Electronic supplementary information (ESI) available: further details of the calculations and structures. See http://www.rsc.org/suppdata/dt/b0/b009596f/

 DOI: 10.1039/b009596f

Table 1 ^{1}H NMR chemical shifts for complexes **1**–**5**

Compound (multiplicity)	H^6 (dd)	H^5 (t)	H^4 (dt)	H^3 (t)	H^7 (s)	CH_3 (s)	$SiMe_3$ (s)	L (multiplicity, *x*H)
1	7.39	6.62	6.38	5.57	2.85	—	0.42	2.20 (s, 3) 2.17 (s, 16) 2.13 (m, 4)
2	7.58	6.71	6.48	5.67	2.70	—	0.48	2.05 (s, 15) 1.94 (s, 8)
3	7.42	6.61	6.45	5.64	2.78	—	0.42	2.02 (s, 12) 1.82 (s, 4)
4	—	6.83	6.54	5.60	2.40	1.81	0.56	2.01 (s, 3) 1.90 (s, 12) 1.66 (m, 8)
5	7.35	6.51	6.47	5.41	3.25	—	0.39	2.53 (d, 18)
rH	8.42	7.06	6.57	6.65	2.28	—	0.02	—
r′H	—	7.30	6.65	6.68	2.26	2.40	0.03	—

Table 2 ^{13}C NMR chemical shifts for complexes **1**–**5**

Compound	C^2	C^6	C^5	C^4	C^3	C^7	CH_3	$SiMe_3$	L
1	169.0	149.4	133.0	116.1	99.8	62.1	—	1.9	59.7 57.3 45.8 42.8
2	168.2	148.9	132.8	115.5	99.9	61.2	—	2.1	57.2 55.2 45.1
3	168.9	148.8	133.5	115.9	100.7	59.9	—	1.7	57.1 45.2
4	153.4	147.5	132.8	113.5	99.4	71.0	25.8	2.3	56.8 53.6 45.4
5	164.3	147.5	131.6	118.3	98.5	69.6	—	1.8	36.6
rH	162.0	149.8	135.4	122.1	119.8	30.1	—	−0.2	—
r′H	160.1	156.1	135.5	118.0	118.0	30.0	24.3	−0.2	—

Results and discussion

All of the complexes, **1**–**5**, were prepared and crystallised, in relatively high yields, in a similar manner, Scheme 1. Metal-

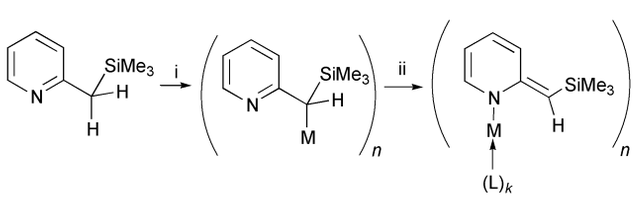

1 M = Na, L = pmdta, *k* = 1, *n* = 2
2 M = K, L = pmdta, *k* = 1, *n* = 2
3 M = Na, L = tmeda, *k* = 1, *n* = 2
4 M = Li, L = pmdta, *k* = 1, *n* = 1
5 M = Mg, L = hmpa, *k* = 2, *n* = 1

Scheme 1 General synthesis of the metal amide complexes **1**–**5**. *Reagents and conditions*: (i) ^{n}BuM (M = Li, Na, K), hexane; Bu_2Mg, heptane; −78 °C to room temperature (ii) *k*L, toluene.

lation was achieved by the addition of **r**H or **r′**H to a hexane suspension of ^{n}BuM, for M = Na, K, or by addition of commercially available hydrocarbon solutions of BuLi (1.6 M in hexane) or $^{n,s}Bu_2Mg$ (1.0 M in heptane) to a hexane solution of the ligand. This invariably resulted in the formation of a dark yellow coloured suspension. Dissolution and complexation was achieved by addition of stoichiometric amounts of the Lewis donor (tmeda, pmdta, hmpa) and subsequent replacement, except for **4**, of the appropriate hydrocarbon by toluene. The solutions at this stage had a much darker orange/red appearance. Single crystals suitable for X-ray diffraction were obtained on cooling the solutions at refrigeration temperature, 4 °C, overnight. All of the crystals, when isolated, proved to be extremely sensitive to atmospheric oxygen and moisture.

The chemical composition of the crystals was determined by elemental analysis, ^{1}H and ^{13}C NMR, in d_6-benzene, and by single crystal X-ray diffraction. The NMR chemical shifts are presented in Tables 1 and 2. As expected, all the metal complexes show a significant downfield shift for both the trimethylsilyl substituted methyl carbon, and the associated proton, on comparison with the conjugate acid of the ligand. This is consistent with an increase in charge on the *ipso*-carbon and subsequent deshielding of the H. However, from these basic ^{1}H and ^{13}C NMR shifts it is not possible to determine absolutely the structure of the complex is solution. A downfield shift for the *ipso*-C*H* has been described to be as a result of the sp^3 to sp^2 change in the *ipso*-C,[5] but comparisons with the complexes [**r**Li·$(Et_2O)]_2$ and [**r**Li·(**R**H)]$_2$, both of which adopt an aza-allylic bonding mode in the solid state, reveals the same tendency, (Me_3SiCH; δ 2.9 and 3.1 respectively). What can be ruled out is that the complexes exist in solution in the carbanion form, *i.e.* with formal M–C bonds. Evidence from ^{1}H–^{7}Li HOESY experiments on dilithiated (*E*)-1,4-bis(trimethylsilyl)-but-2-ene and (*E*)-1,4-bis(trimethylsilyl)-2,3-dimethylbut-2-ene indicated that two complexes existed as metal bridged carbanions, and not as delocalised species, with the charge localised on the 1,4 carbons. This causes the associated protons to become more shielded, leading to a shift in the signals to a higher frequency than seen in the non-metallated but-2-enes[6] whereas formation of olefinic character, consistent with aza-allyl or amide formation in **1**–**5**, should have achieved the opposite effect.

One point of interest in comparing the NMR shifts is the higher frequency shifts for the *ipso*-carbon (C^7) and proton (H^7) in the Mg complex (see Fig. 2 for the NMR numbering scheme adopted). It would seem to indicate greater polarising power of Mg over that of the heavier alkali metals. However, it may be possible to account for this discrepency based on the change in donor ligand from N-based, tmeda, pmdta, to the O based hmpa, the O atom of which carries significant negative charge.

Table 3 Selected bond lengths (Å) and angles (°) for complex **1**, [**r**Na·(pmdta)]$_2$

Na–N(1)	2.475(3)	Na–N(07)	2.618(4)
Na–N(1′)	2.586(3)	N(1)–C(2)	1.388(4)
Na–N(01)	2.669(3)	N(1)–C(6)	1.332(6)
Na–N(04)	2.601(3)	C(2)–C(21)	1.364(6)
Na–H(21)	3.07(2)	Na–H(21′)	3.12(3)
N(1)–Na–N(1′)	91.24(8)	N(04)–Na–N(1′)	163.7(1)
N(1)–Na–N(01)	106.1(1)	N(07)–Na–N(1′)	93.9(1)
N(1)–Na–N(04)	98.22(9)	N(01)–Na–N(04)	69.49(9)
N(1)–Na–N(07)	137.8(1)	N(01)–Na–N(07)	107.0(1)
N(01)–Na–N(1′)	120.57(9)	N(04)–Na–N(07)	70.2(1)
Na–N(1)–Na′	88.76(9)	Na–N(1)–C(2)	115.2(2)
N(1)–C(2)–C(21)	121.0(3)	Na–N(1)–C(6)	107.6(2)
C(2)–N(1)–C(6)	118.9(3)		

Table 4 Selected bond lengths (Å) and angles (°) for complex **2**, [**r**K·(pmdta)]$_2$

K–N(1)	2.839(6)	K–N(07)	2.910(8)
K–N(1′)	2.824(7)	N(1)–C(2)	1.36(1)
K–N(01)	2.89(1)	N(1)–C(6)	1.36(1)
K–N(04)	2.876(8)	C(2)–C(21)	1.38(1)
K–H(21)	2.83(5)	K–H(21′)	3.00(5)
N(1)–K–N(1′)	90.8(2)	N(04)–K–N(1′)	161.8(2)
N(1)–K–N(01)	104.2(3)	N(07)–K–N(1′)	100.9(2)
N(1)–K–N(04)	106.3(2)	N(01)–K–N(04)	60.7(3)
N(1)–K–N(07)	139.7(2)	N(01)–K–N(07)	101.9(3)
N(01)–K–N(1′)	121.7(3)	N(04)–K–N(07)	62.0(2)
K–N(1)–K′	89.2(2)	K–N(1)–C(2)	95.6(5)
N(1)–C(2)–C(21)	122.7(7)	K–N(1)–C(6)	118.9(6)
C(2)–N(1)–C(6)	118.5(7)		

Table 5 Selected bond lengths (Å) and angles (°) for complex **3**, [**r**Na·(tmeda)]$_2$

Na(2)–N(1)	2.51(1)	N(1)–C(2)	1.38(2)
Na(1)–N(1)	2.39(1)	N(1)–C(6)	1.34(2)
Na(2)–N(02)	2.40(2)	C(2)–C(21)	1.37(2)
Na(1)–N(01)	2.45(1)	Na(1)–H(21)	2.58(8)
Na(2)–H(21)	2.74(8)		
N(1)–Na(2)–N(1′)	95.2(4)	N(1)–Na(1)–N(1′)	101.3(4)
N(1)–Na(2)–N(02)	100.8(5)	N(1)–Na(1)–N(01)	116.5(5)
N(1)–Na(2)–N(02′)	150.7(5)	N(1)–Na(1)–N(01′)	123.7(5)
N(01)–Na(1)–N(01′)	75.8(5)	N(02)–Na(2)–N(02′)	76.6(6)
Na(2)–N(1)–C(2)	95.6(8)	Na(2)–N(1)–C(2)	108.4(8)
Na(2)–N(1)–C(6)	123(1)	Na(2)–N(1)–C(6)	122(1)
N(1)–C(2)–C(21)	121(1)	C(2)–N(1)–C(6)	118(1)

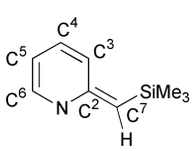

Fig. 2 NMR numbering scheme.

Crystallographic studies

All of the complexes, **1**–**5**, adopt the enamide form of the anion in the solid state. They are contact ion pairs with formal N–M bonds and an exocyclic double bond from C^2 to the *ipso*-carbon, C^7 (**1**, 1.364(6); **2**, 1.38(1); **3**, 1.37(2); **4**, 1.393(4); **5**, 1.36(1), 1.37(1) Å). As such they are all, formally at least, metal amides in the solid state. Important bond lengths and angles are given in Tables 3 to 7. The complexes containing the larger alkali metal cations, Na (**1**) and K (**2**), are dimeric, even with the bulky tridentate ligand, pmdta. In all cases the pmdta ligands use all three available N centres in bonding to the metal. The Li and Mg complexes, (**4** and **5**), are, in contrast, monomeric, presumably since the metal centre achieves a stable coordination environment without the need for dimer formation.

Table 6 Selected bond lengths (Å) and angles (°) for complex **4**, [**r**′Li·(pmdta)]

Li–N(1)	2.044(5)	N(1)–C(1)	1.396(4)
Li–N(2)	2.162(5)	N(1)–C(5)	1.348(4)
Li–N(3)	2.267(6)	C(1)–C(7)	1.393(4)
Li–N(4)	2.120(6)		
Li–H(21)	2.22(est.)		
N(1)–Li(1)–N(2)	110.6(2)	N(2)–Li(1)–N(3)	83.3(2)
N(1)–Li(1)–N(3)	156.4(3)	N(2)–Li(1)–N(4)	122.4(3)
N(1)–Li(1)–N(4)	103.3(2)	N(3)–Li(1)–N(4)	83.4(2)
Li(1)–N(1)–C(1)	98.7(2)	Li(1)–N(1)–C(5)	132.2(3)
C(1)–N(1)–C(5)	119.9(2)	N(1)–C(1)–C(7)	119.4(3)

Table 7 Selected bond lengths (Å) and angles (°) for complex **5**, [(**r**)$_2$Mg·(hmpa)$_2$]

Mg–O(1)	1.943(5)	Mg–N(31)	2.057(6)
Mg–O(2)	1.919(6)	Mg–N(41)	2.071(5)
Mg–H(321)	2.7_5	Mg–H(421)	2.7_3
O(1)–P(1)	1.476(5)	O(2)–P(2)	1.475(6)
N(31)–C(32)	1.413(7)	C(32)–C(321)	1.36(1)
N(41)–C(42)	1.393(9)	C(42)–C(421)	1.37(1)
O(1)–Mg–O(2)	105.2(2)	N(31)–Mg–N(41)	110.5
O(1)–Mg–N(31)	112.0(2)	Mg–O(1)–P(1)	157.4(4)
O(1)–Mg–N(41)	103.7(2)	Mg–O(2)–P(2)	167.4(3)
O(2)–Mg–N(31)	113.6(2)	N(31)–C(32)–C(321)	121.4(6)
O(2)–Mg–N(41)	111.3(2)	N(41)–C(42)–C(421)	119.8(5)
Mg–N(31)–C(32)	123.1(4)	Mg–N(31)–C(36)	116.2(4)
Mg–N(41)–C(42)	124.5(4)	Mg–N(41)–C(46)	116.6(5)

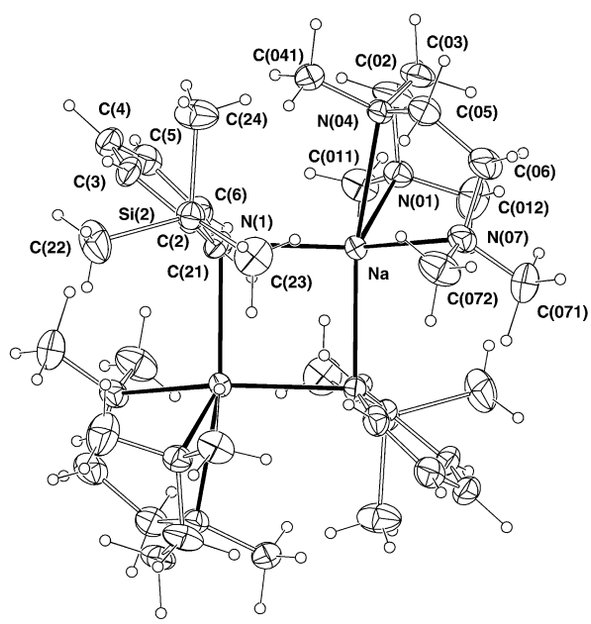

Fig. 3 Molecular structure of [**r**Na·(pmdta)]$_2$, **1**.

Complex **1**, [**r**Na·(pmdta)]$_2$, crystallises in the space group $P2_1/c$, with two molecules (dimers) in the unit cell. As can be seen in the molecular structure, Fig. 3, the dimer is disposed about a centre of inversion and as a result the central feature of the complex is a planar four membered (NNa)$_2$ ring about which the ligands and the pmdta moieties adopt a *trans* configuration. This conformation is probably the most common arrangement found for complexed sodium amides in the solid state.[7] In fact, the same structural feature is evident in **3**, [**r**Na·(tmeda)]$_2$, Fig. 4. The dimeric unit on this occasion has a C_2 rotation axis through the two Na centres consistent with the ligands, again, being *trans* about the ring. The two tmeda molecules, though, adopt an unsymmetrical arrangement in relation to the (NNa)$_2$ ring plane. The environments of the two

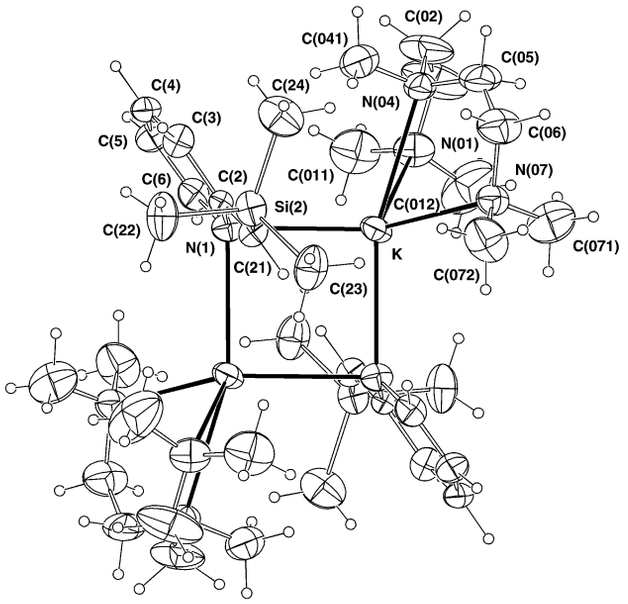

Fig. 4 Molecular structure of [**r**K·(pmdta)]$_2$, **3**.

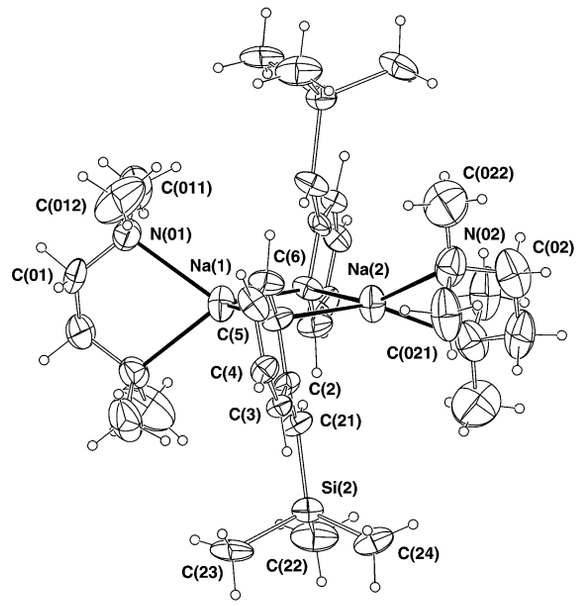

Fig. 5 Molecular structure of [**r**Na·(tmeda)]$_2$, **2**.

metal atoms differ considerably, principally because of a difference in the twists of the (tmeda)N_2Na planes *vis-à-vis* the $Na_2N(1)_2$ plane: the $(N(01))_2Na/Na(N(1))_2$ interplanar dihedral angle about Na(1) is 83.5(5)° whereas that for $(N(02))_2Na/Na(N(1))_2$ about Na(2) is 41.5(6)°, the environment of Na(2) being 'flatter' or more nearly planar than tetrahedral. The two tmeda ligands are of the same chirality. This structural arrangement is most likely a result of crystal packing forces since the structure of **1** suggests that the ligands can orientate themselves to accommodate an even larger donor ligand with concomitant increase in coordination at the metal centre, *i.e.* 5 in **1** and 4 in **3**. Given the essentially planar nature of the anion, constrained by the pyridyl ring and exocyclic double bond, a good comparison can be made between **1** and **3** and the dimeric sodium indole complexes, [$(C_6H_4)C_2NNa$·(pmdta)]$_2$, **6**, and [$(C_6H_4)C_2NNa$·(tmeda)]$_2$, **7**.[8] The $(NaN)_2$ rings in both **1** and **6** have internal angles about, or approaching, an ideal right angle; N(1)–Na–N(1′) in **1** is 91.24(8) and in **6** N(1)–Na–N(1a) is 90.1°, though an analysis of the bond lengths reveals that the ring in **1** is, in fact, rectangular, Na–N(1) and Na–N(1′) are 2.475(3) and 2.586(3) Å respectively, while in **6** it is almost a perfect square, Na–N(1) and Na–N(1a), 2.474(4) and 2.481(5). The coordination to the metal by all three available N atoms of pmdta renders the Na cationic centres five coordinate in both complexes, with the bond distances being comparable and highlighting the tendency to short, intermediate and long bonds. In **1** and **6** these are 2.601(3), 2.618(4), 2.669(3) and 2.559(4), 2.608(5), 2.623(5) Å respectively. The slightly longer bonds in **1** may be accounted for by the added steric effects of the Me_3Si group.

The range of N_{amido}–Na bond distances in **3** (Na(2)–N(1) 2.51(1), Na(1)–N(1) 2.39(1) Å) and in **7** (Na–N(1) 2.478(5), Na–N(1a) 2.356(5) Å) indicate that the $(NNa)_2$ ring cores are much more akin to the rectangular nature of **1** than of **6**. The shortening of the bond lengths in **3** relative to **1**, almost certainly results from the lower, four coordinate state of the Na cation. An examination of the internal angles reveals also that there is a pronounced move away from almost ideal right angles towards a more rhomboidal structure. Thus the internal angles at the metal centres in **3** are 95.2(4)° (N(1)–Na(2)–N(1′)) and 101.3(4)° (N(1)–Na(1)–N(1′)), which are slightly more obtuse than those in **6** (92.9°). An interesting feature of the structure of **6** which is not present in **7** is the agostic interaction the Na centre has with a C adjacent to the N_{amido}, which causes the indole moieties to tilt. This raises the effective coordination of the metal and compensates for the relatively low formal coordination environment of four. The Na–H(21, 21′) distances in **1** of 3.07(2) and 3.12(3) Å, are significantly different from comparative distances in **3**, Na(1)–H(21) 2.58(8) and Na(2)–H(21) 2.74(8) Å, indicating that there are relatively strong compensatory agostic interactions in **3**, similar to those observed in **6**. This is much less pronounced in **1**, especially when compared with those in the K analogue, **2**, (see below), and is clearly a result of increased steric crowding. The environment about Na(2) in **3** has a notably large angle (N(02)–Na(2)–N(1′)) (150.7(5)°) and the difference might be sought in an approach of H(21) to the coordination sphere here.

Complex **2**, [**r**K·(pmdta)]$_2$, shown in Fig. 5, is only 'isomorphous' with its Na analogue **1** and not isostructural despite having similar cell dimensions, being in the same space group ($P2_1/n$), and with the dimer disposed about the same site symmetry. In detail the structures differ in the inclination of the anions to the M_2N_2 core plane in terms of the relative projections of the silyl substituted methyl, C(23), over that plane. More subtly, although the dispositions of N(01, 04, 07) *vis-à-vis* that plane are similar in the two complexes, N(04, 07) lie to one side of the methyls C(041, 072) straddling the $SiMe_3$, equatorial and axial to the normal of the core respectively, in the sodium complex, but, in the complex of the larger potassium, both are 'axial', accompanied by concomitant changes in the conformations of the $(CH_2)_2$ linkages.

The central four membered planar $(NM)_2$ ring on this occasion, however, resembles more closely that of **6** rather than **1** in being almost a perfect square, with K–N_{amido} distances of 2.839(6) (K–N(1)) and 2.824(7) Å (K–N(1′)) and an internal angle at the metal centre of 90.8(2)°. The ligands again adopt the more energetically favourable *trans* position relative to the ring. The K cations become formally five coordinate on bonding with the three available N atoms of pmdta. However, the metal increases its coordination environment by forming an agostic interaction with the *ipso*-H, K–H(21) 2.83(1) Å. This is shorter than the comparative distances in the Na analogue, **1**, resulting from the larger cation and consequent reduction in steric crowding. The agostic distances in **2** are consistent with similar interactions observed in $[(^iPr)_2NK(tmeda)]_2$ av. 2.89 Å.[9] All the K–N distances in the structure are comparable with other analogous published structures; *cf.* [(2-Pyr)$(Ph)_2$CK·(pmdta)(thf)], K–N_{amido} 2.809(5) Å.[4]

Complex **4**, [**r′**Li·(pmdta)], crystallises in the space group $P2_1/n$ with one formula unit devoid of crystallographic

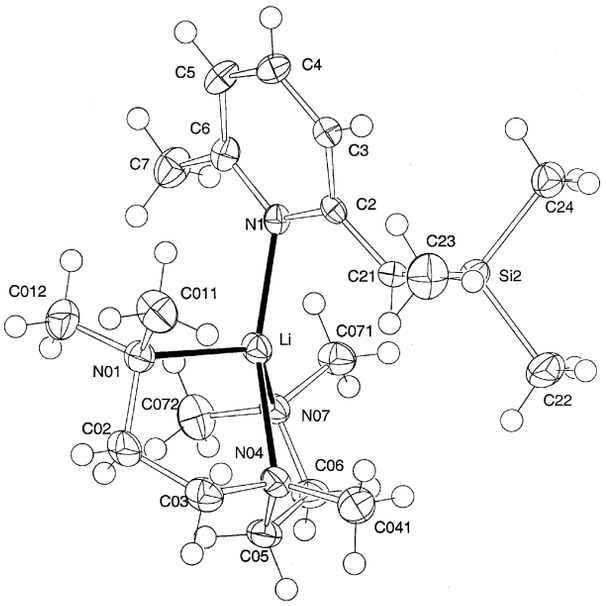

Fig. 6 Molecular structure of [**r**′Li·(pmdta)], **4**.

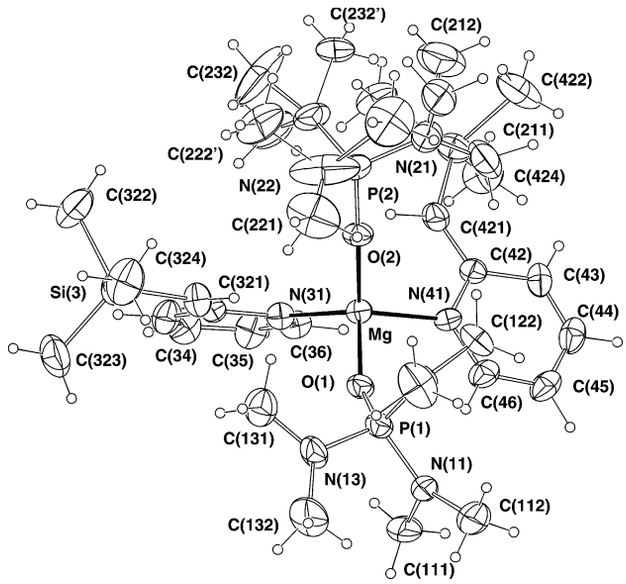

Fig. 7 Molecular structure of $[(\mathbf{r})_2Mg\cdot(hmpa)]_2$, **5**.

symmetry comprising the asymmetric unit. The smaller cation size and lower coordinative demands of Li means that the structure is monomeric rather than dimeric, as shown in Fig. 6. The presence of additional steric bulk in the ligand with the Me in the 6-position of the pyridyl ring is unlikely to be a significant determining factor in this. All tetra-coordinate Li amide complexes incorporating pmdta are monomeric,[10] the exceptions being the limited ladder structures based on the pyrrolidinyl ligand[11] and the unusual trimetallic complex, $[(PhNHLi)_3\cdot(pmdta)_2]$.[12] The Li cation in **4** is in an extremely distorted tetrahedral environment with the ligand forcing the pmdta to adopt an orientation which leaves what appears to be an open coordination face at the metal centre, indicated by the N(1)–Li–N(3) angle of 156.4(3)°. This is most likely a result of the presence of the Me_3Si group, however, one result (or additional cause?) is that Li forms, as with the Na and K analogues, a close agostic interaction with the *ipso*-C*H*, Li–H(21) 2.22 Å. This distance is appreciably shorter than the reported agostic interactions, averaging 2.66 Å, in $[(PhCH_2)_2NLi]_3$.[13] All of the N–Li bond distances are within the range established for similar lithium amide complexes.

Complexes **1**–**4**, and the other Li examples quoted above, have established that the internal alkyl to amide rearrangement is facile and apparently energetically favourable for the alkali metals. It was of interest to us to observe whether a Group 2 metal would give rise to similar behaviour given that the less electropositive metals give solely alkyl complexes.[14] We therefore made the bis-solvated magnesium amide, **5**, $[(\mathbf{r})_2Mg\cdot(hmpa)_2]$ which crystallises in the space group $P2_1/c$ one formula unit, devoid of crystallographic symmetry, comprising the asymmetric unit of the structure. As shown in Fig. 7, the structure is monomeric and the alkyl to amide rearrangement has occurred. The coordination environment of the Mg cation is tetrahedral, the metal forming two formal N_{amido}–Mg bonds and being solvated by two hmpa molecules. However, considerable asymmetry is observed in each ligand in the angles to either side of the Mg–N bond. The trend away from using hmpa in such reactions meant that we used it only as a last resort since we were unable to obtain crystals with any other of the common N and O based donors, mainly as a result of low solubility. There are surprisingly few hmpa complexes of magnesium amides of the structural type adopted by **5**. Two which are useful for comparison are $\{[(PhCH_2)_2N]_2Mg\cdot(hmpa)_2\}$, **8**,[15] $\{[(Mes)NH]_2Mg\cdot(hmpa)_2\}$ (Mes = 2,4,6-trimethylbenzene), **9**.[16] The two Mg–N bonds in **5** (Mg–N(31) 2.057(6), Mg–N(41) 2.071(5) Å) are comparable in distance with those in **9** (2.006(10), 2.022(10) Å), but are slightly longer than those in **8** (1.980(5), 1.976(4) Å). In contrast, the Mg–O bonds in **5**, Mg–O(1), 1.943(5), Mg–O(2), 1.919(5) Å, are significantly shorter than those in **8** and **9**, 1.975(4), 1.967(3) and 1.965(8), 1.980(8) Å respectively. Since the Mg–O bonding is essentially electrostatic in nature, due in part to the high charge separation in the P^+–O^- bond in hmpa, any variation in bond length can be understood in terms of the steric interaction of ligands and donors and the attainment of the most energetically stable conformation in the molecule. This, in conjunction with crystal packing forces, most likely accounts for the lack of symmetry in the molecule in the solid state, highlighted by the different Mg–O–P angles of 157.4(4) and 167.4(3)°, which is not observed in solution on the NMR timescale. One point of interest is whether the Mg forms agostic interactions with the *ipso*-H. We are unaware of any reports in the literature of Mg being involved in agostic bonding. However, the bond distances of av. 2.7 Å (est.) for Mg–H(321, 421) are certainly indicative of such interactions in the light of comparative bonding distances described for Li, and especially since Mg is a slightly larger cation.

Ab initio calculations

We have employed *ab initio* MO calculations[17] to examine the electronic structures and energies of **r**H, the metallated derivatives **r**Li, **r**Na, and $(\mathbf{r})_2Mg$ and some simple solvated compounds of the metallated species in order to investigate the mode of bonding of the metallic ions Li^+, Na^+ and Mg^{2+} with the ligand **r** and to ascertain how the presence of a donating solvent affects the nature of the interaction between the metallic cation and the possible anionic centres on **r**. The geometry optimisations were carried out at the Hartree–Fock level using the 6-31G* basis set.[18] Calculations and geometry optimisations on the parent hydrocarbon (**I**, **II**) and the complexes formed with the alkyl metal reagents prior to metallation occurring (**IIIa–c**, **IVa**,**b**) are given in the supplementary data, along with the calculated energies for all the model complexes.†

Five possible models of **r**Li (**Va**–**e**) were examined. The first two models considered the lithium to bond to **r** *via* the aza-allyl (see Fig. 1) π-electronic system: for model (**a**) the $SiMe_3$ portion lies *cis* to the C^2–N bond and for model (**b**) it is positioned *trans*. The next two models invoked the enamide description of **r** and here Li bonds only to N *via* the σ-electron framework. The presence of the double bond (C^2–C^7) allows two possible configurations: for model (**c**) the C^7–$SiMe_3$ bond is *cis* to the

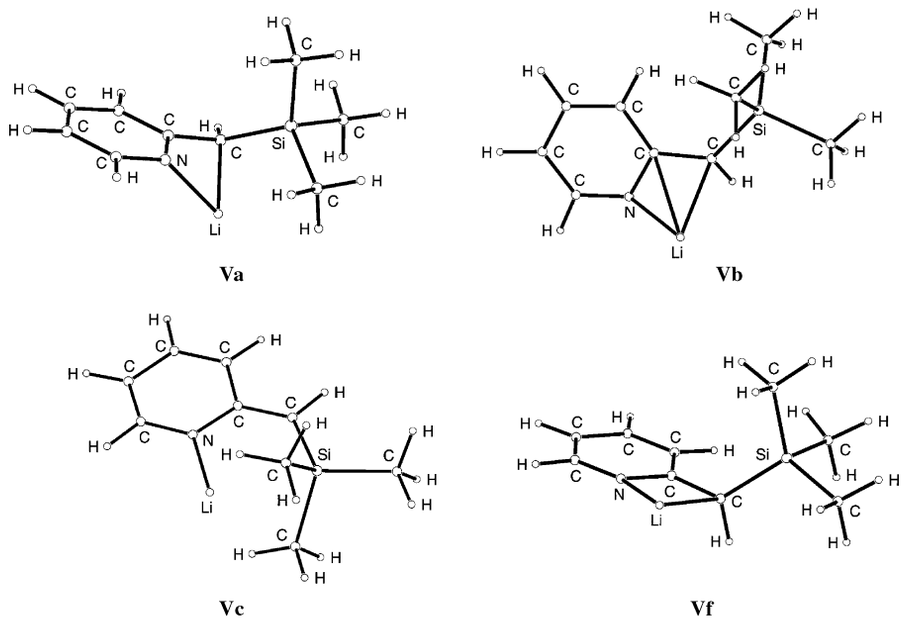

Fig. 8 Optimised geometries of **r**Li; *cis* aza-allyl (**Va**), *trans* aza-allyl (**Vb**), enamide (**Vc**) and intermediate (**Vf**).

N–C^2 bond and for model (**d**) this bond lies *trans*. The fifth model looked at the carbanion representation of **r** and was constructed with Li forming a σ-bond directly to C^7.

The most stable species after the geometry optimisation process is **Va** (see Fig. 8) which has Li lying below an extension of the plane containing the aza-allyl unit and bonding to each of the three atoms. The resulting bond lengths are Li–N 1.940, Li–C^2 2.241, and Li–C^7 2.097 Å indicating moderately strong bonding to all three atoms. As the lithium is interacting with the π-electronic system of the aza-allyl moiety, the bond lengths of the latter have altered from the values found for **r**. The C^2–C^7 bond distance has increased to 1.428 Å while the C^2–N bond length has shortened to 1.357 Å; both changes are indicative of reduced π-electron conjugation. An interesting feature of the structure is that a Si–Me bond almost eclipses the C^7–Li bond due to a weak interaction (at 2.48 Å) between the lithium and a negatively charged carbon of the methyl group.

The second model (**Vb**) is 3.2 kcal mol^{-1} less stable than **Va**. It has the same gross features as **Va** except there is no secondary interaction of Li with the $SiMe_3$ moiety. Therefore the Li bonds more strongly to the aza-allyl unit than it does in **Va** and in particular the Li–N and Li–C^7 bonds are slightly shorter (by ≈0.02 Å).

The third model (**Vc**) which has Li bonding solely to the lone pair of electrons on N is 12.4 kcal mol^{-1} less stable than **Va**. The optimised geometry has the Li–N bond of length 1.888 Å lying in the same plane as the pyridine ring and the C^2–C^7 bond. In this model the $SiMe_3$ group lies *cis* to the C^2–N bond and is adjacent to the N–Li bond. This allows the carbons from two Me groups to provide additional stabilising interactions with the Li and the resulting two C–Li bonds are equal and span 2.5 Å.

The fourth model (**Vd**) was initially set up in the same manner as **Vc** except for the alternative positioning of the $SiMe_3$ and H groups about C^7. On optimisation the Li in the absence of any secondary stabilising bonding with the $SiMe_3$ group migrated to bond to the aza-allyl moiety and gave the structure of **Vb**. In a similar manner when the optimisation was carried out on the fifth model (**Ve**) the Li which was originally bonded only to C^7, moved to bond also with the N and ultimately gave the same geometry as that of **Va**.

In summary the more stable bonding modes of Li with **r** involve the interactions with the aza-allyl unit. It was of interest to determine the energy required to inter-convert the structures with this bonding feature. The calculated energy for the intermediate (**Vf**, see Fig. 8) is 7.1 kcal mol^{-1} higher in energy than **Va** and 3.9 kcal mol^{-1} less stable than **Vb**. Hence interconversion would not be too difficult to achieve especially for the transformation of **Vb** to **Va**. The interesting feature of the structure of **Vf** is that the atoms N, C^2, C^7, and Li, form a four-membered ring which lies almost coplanar with the pyridine ring. The C^7–H and the C^7–$SiMe_3$ bonds are situated perpendicular to the ring and rotation of these bonds will produce either **Va** or **Vb**, Fig. 8.

Calculations on **r**Na employed five models (**VIa**–**e**) based on those used for **r**Li and the same trends were found with regard to the structures and the energies. Thus the most stable structure (**VIa**) has Na bonded to the atoms of the aza-allyl unit (Na–N 2.371, Na–C^2 2.611, Na–C^7 2.454 Å) and also engaged in additional bonding to a carbon of the $SiMe_3$ unit (Na–C 2.76 Å). The sister structure **VIb** is 2.8 kcal mol^{-1} less stable and is characterised by Na bonding only to the atoms of the aza-allyl unit. The transition state between **VIa** and **VIb** is found to be 5.4 kcal mol^{-1} less stable than **VIa.** Model **VIc** which contains a Na–N σ-bond of length 2.247 Å and agostic type bonds to two carbon atoms of the $SiMe_3$ group (Na–C 2.71 Å) is 11.0 kcal mol^{-1} less stable than **VIa**. Optimisation of the structures **VId** and **VIe** resulted in geometries which are identical to those of models **VIb** and **VIa** respectively.

Calculations on $\mathbf{r}_2$Mg employed seven models (**VIIa**–**g**). The first four models invoked the aza-allyl description of **r**. In **VIIa** the Mg was bonded to both aza-allyl units so that the coordinating atoms N and C^7 of both **r** moieties lie in the same plane as the Mg. In models **VIIb**–**d** the coordinating atoms of the aza-allyl units were arranged in tetrahedral fashion about Mg with the different arrangement of the groups about the C^7 atoms resulting in the three models. For model **VIIb** the groups about the two C^7 atoms were organised as (*R*,*S*) while the corresponding (*R*,*R*) and (*S*,*S*) arrangements were present in **VIIc** and **VIId** respectively. In models **VIIe** and **VIIf** the magnesium was bonded to both N atoms *via* a linear σ-bond and the two pyridine rings were roughly in the same plane. The differing placements of the $SiMe_3$ groups with regard to the C^2–C^7 double bond allowed the *trans* arrangement with regard to the C^2–N bond to be present in **VIIe** and the *cis* arrangement to be found in **VIIf**. Model **VIIg** was constructed with the **r** moieties linked to the Mg atom *via* a linear C^7–Mg–C^7 unit.

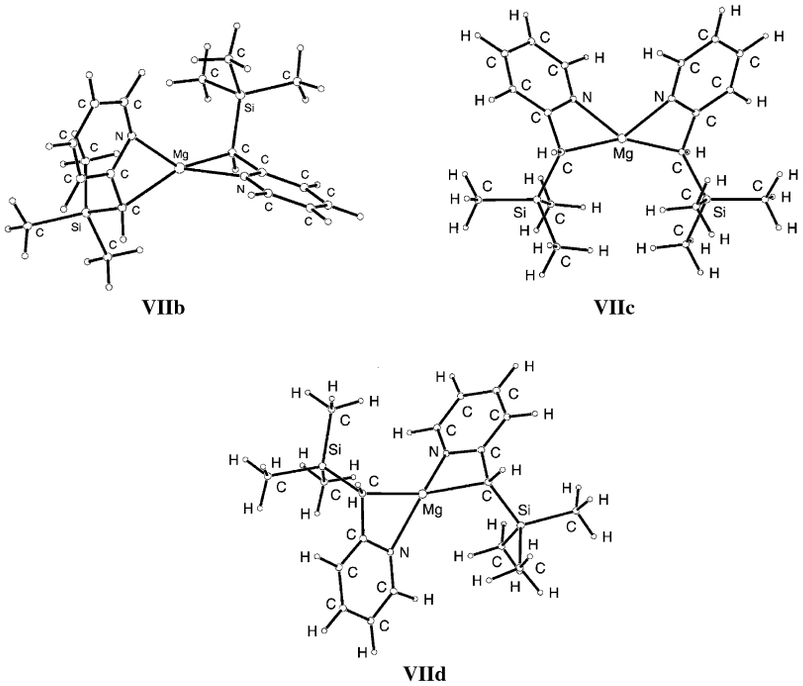

VIIb **VIIc**

VIId

Fig. 9 Optimised geometries of three possible arrangements for aza-allylic $\mathbf{r}_2$Mg; *R*,*S* (**VIIb**), *R*,*R* (**VIIc**) and *S*,*S* (**VIId**).

The tetrahedral arrangement of the aza-allyl groups was found to be the most stable (**VIIb–d**), Fig. 9, and this was also obtained during the optimisation of models **VIIe** and **VIIg**. The *RS* and *RR* models gave almost identical energies (difference is less than 0.01 kcal mol^{-1}) while the *SS* model is 0.3 kcal mol^{-1} less stable. All three models consist of an almost perpendicular arrangement of the two aza-allyl units about Mg giving a distorted tetrahedral arrangement of Mg–C^7 and Mg–N bonds. The Mg lies slightly below both planes extending from the pyridine rings. The torsion angle for Mg–N–C^2–C^7 is ≈15° while the corresponding value for the Li–N–C^2–C^7 in **Va** is ≈30°. This means that compared to **Va** there is less π-orbital involvement and more σ-orbital participation in the bonding between the aza-allyl units and Mg (C^7–Mg 2.191 and N–Mg 2.181 Å). Thus there is very little interaction of the orbitals of C^2 with those of Mg and this results in a Mg–C^2 distance of 2.564 Å. The C^2–C^7 bond length of 1.485 Å reflects that there is very little π bonding present in this bond while the C^2–N bond distance of 1.342 Å indicates a double bond and cessation of π conjugation along the N–C^2–C^7 sub-unit. Models **VIIa** and **VIIf** optimised to give energy minima with the same gross features as their original geometry but the subsequent frequency analyses revealed that they were not true minima and so they will not be discussed further.

In conclusion, the bonding in the species **r**Li, **r**Na and $\mathbf{r}_2$Mg can be described in terms of the interaction of the metallic cation with atoms N, C^2, and C^7 of the aza-allyl portion of **r** with a reduction in the π-electronic conjugation within this region. The energies of all three reactions (given by eqn. 1)

$$n\,\mathbf{r}H + M(CH_3)_n \longrightarrow M\mathbf{r}_n + n\,CH_4 \qquad (1)$$

to produce these species can be estimated by using the SCF energies of the reactants and products. The calculations show that each reaction is exothermic with $\Delta E = -31.4$ kcal mol^{-1} (for M = Li), −29.0 kcal mol^{-1} (for M = Na), and −41.4 kcal mol^{-1} (for M = Mg).

The next step in the theoretical investigation was to examine how the coordination of donor solvents to the metal ion affected the mode of bonding of the metal to **r**. In the case of **r**M where M = Li and Na, this was carried out by systematically adding one and two molecules of NH_3 and then a molecule of pmdta to the metal ion. For the corresponding magnesium compound, $\mathbf{r}_2$Mg, the effect of addition of two molecules of water (modelling the donor solvent hmpa) to Mg was similarly investigated.

Five models of **r**Li·NH_3 were constructed (**VIIIa–e**), along similar lines to those of (**IVa–e**) and their geometries were optimised. The most stable structure was **VIIIa**, Fig. 10, where Li is bonding principally to the N, C^2 and C^7 atoms of the aza-allyl portion and the N atom of NH_3, as well as interacting weakly with a methyl carbon of the $SiMe_3$ group. The effect of the presence of the NH_3 is to weaken the interaction of Li with the **r** moiety and thus to lengthen the Li–N bond (to 1.987 Å), the Li–C^2 bond (to 2.260 Å), the Li–C^7 bond (to 2.157 Å) and the Li···CH_3 distance (to 2.70 Å). In the aza-allyl portion of **r**, the C^2–N bond has increased to 1.358 Å while the C^2–C^7 bond has shortened to 1.422 Å, therefore conjugation in the aza-allyl section has slightly increased by the addition of the donor solvent to Li. The Li–N coordinating bond length is 2.071 Å and the calculated energy of complexing is −22.2 kcal mol^{-1}.

Model **VIIIb** is less stable than **VIIIa** by 2.0 kcal mol^{-1} although the energy of complexing is −23.4 kcal mol^{-1} and this latter value reflects the less congested situation about Li compared with that in **VIIIa**. The complexing of **VIb** by NH_3 has weakened and lengthened the Li–aza-allyl interactions. Model **VIIIc** which is 10.4 kcal mol^{-1} higher in energy than **VIIIa** has lithium bonded to the N of NH_3, the N of **r**, and to two carbons of the $SiMe_3$ group in a distorted tetrahedral situation. Models **VIIId** and **VIIIe** on geometry optimisation gave structures identical to models **VIIIb** and **VIIIa** respectively.

Five models of **r**Na·NH_3 were formed (**IXa–e**), and the geometry optimisation process replicated the findings of the lithium series. In summary, the most stable model (**IXa**) contains the aza-allyl representation of **r** whose interactions to Na have all been weakened by NH_3 coordination to yield Na–N (2.352 Å), Na–C^2 (2.624 Å), and Na–C^7 (2.508 Å). The Na–N coordinate bond spans 2.432 Å and the resulting energy of complexing is −18.0 kcal mol^{-1}. Models **IXb** and **IXc** are less stable than **IXa** by 2.2 kcal mol^{-1} and 9.4 kcal mol^{-1} respectively.

A similar exercise was carried out for **r**Li·$(2NH_3)_2$ (**Xa–e**), and **r**Na·$(2NH_3)_2$ (**XIa–e**). For models **a** and **c** the presence of an extra donor molecule bonded to the metal ion causes steric

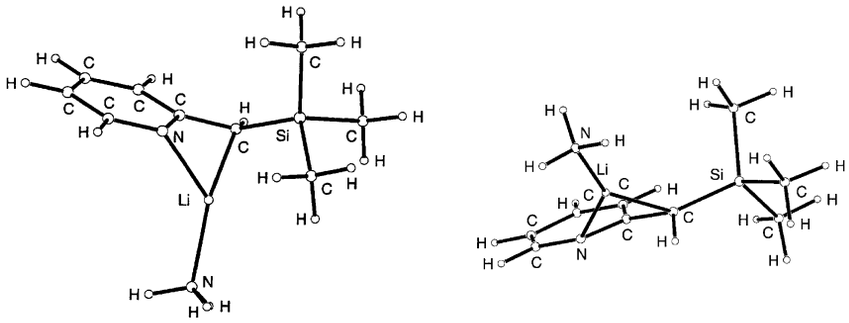

VIIIa **VIIIb**

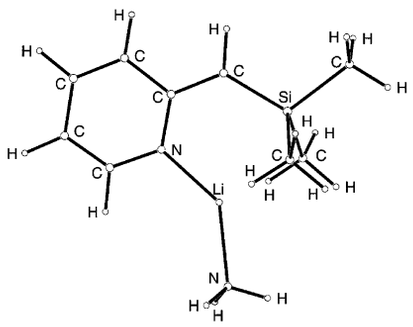

VIIIc

Fig. 10 Optimised geometries of [**r**Li·NH_3] (**VIIIa**–**c**).

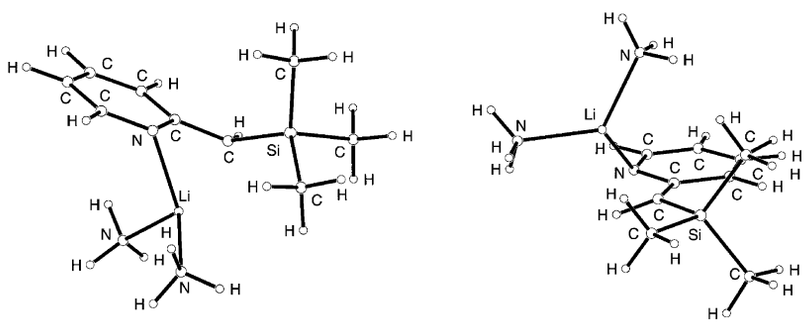

Xa **Xb**

Fig. 11 Optimised geometries of [**r**Li·$(NH_3)_2$] (**Xa**,**b**).

congestion due to the juxtaposition of the bulky $SiMe_3$ group. For this reason model **a** in the lithium series is no longer the most stable structure being 1.5 kcal mol^{-1} higher in energy than model **b**, Fig. 11. For the sodium counterparts, model **a** is still the preferred structure but by a mere 0.6 kcal mol^{-1}. Here the longer bonds emanating from sodium will result in less steric repulsion between the donor molecules and neighbouring groups. For both series model **c** does not optimise to a unique geometry because the presence of donor molecules lessens the influence of the secondary attraction between the metal and the carbon atoms of the $SiMe_3$ group. The metal ions move to participate in aza-allyl bonding and a geometry identical to that of model **a** results. For models **d** and **e**, the metal is initially coordinated to only three groups and therefore the metal ion migrates during the geometry optimisation process to increase its coordination and this results in a geometry indistinguishable from that of models **b** and **a** respectively. The effect of the coordination of the second NH_3 to the metal is to further weaken and lengthen the **r**–M interactions with the concomitant increase in the π-electronic conjugation through the N–C^2–C^7 portion. The energies of complexing of two NH_3 molecules with the **r**M species are −38.8 kcal mol^{-1} (M = Li) and −31.5 kcal mol^{-1} (M = Na).

Three models of **r**Li·pmdta (**XII**), Fig. 12, and **r**Na·pmdta (**XIII**) were constructed. It was found that construction of models of type **a** and **c** was not possible as realistic coordination of pmdta to the metal ion was prevented by the presence of the neighbouring bulky $SiMe_3$ group. Hence only models **b**,**d** and **e** were optimised. The most stable structure of **r**Li·pmdta was found to be **XIId**, which was based on the enamide representation of **r**. Li is bonded to the **r** moiety solely *via* a Li–N bond of length 1.984 Å which lies roughly in the same plane as the pyridine ring and the C^2–C^7 bond. The non-interaction of C^2 and C^7 with Li has meant that the N–C^2–C^7 portion has reverted to the aza-allyl distances found in **r** (**II**) *i.e.* C^2–C^7 1.389 and C^2–N 1.373 Å. This geometrical set-up of groups about C^7 ensures that the hydrogen bonded to C^7 is pointing towards the Li and in this case it is 2.34 Å away from the Li. The pmdta bonds to the Li *via* three Li–N bonds of length 2.145, 2.189 and 2.282 Å and the resulting energy of complexing is −29.4 kcal mol^{-1}. **XIIb**, which is less stable than **XIId** by 1.1 kcal mol^{-1}, originally had the Li bonding to the aza-allyl portion of **r**. After optimisation the Li is still lying below a plane containing the pyridine ring, but the interaction of Li with C^2 and C^7 is now weak (*e.g.* Li–C^7 2.607 Å). Furthermore, examination of the N–C^2–C^7 portion reveals that aza-allyl conjugated π-bonding is present (C^2–C^7 1.398, N–C^2 1.368 Å). The hydrogen bonded to C^7 is 2.28 Å from the Li. There are four Li–N bond lengths; the strongest is to the pyridine ring (2.038 Å) while the three pmdta coordinate bonds

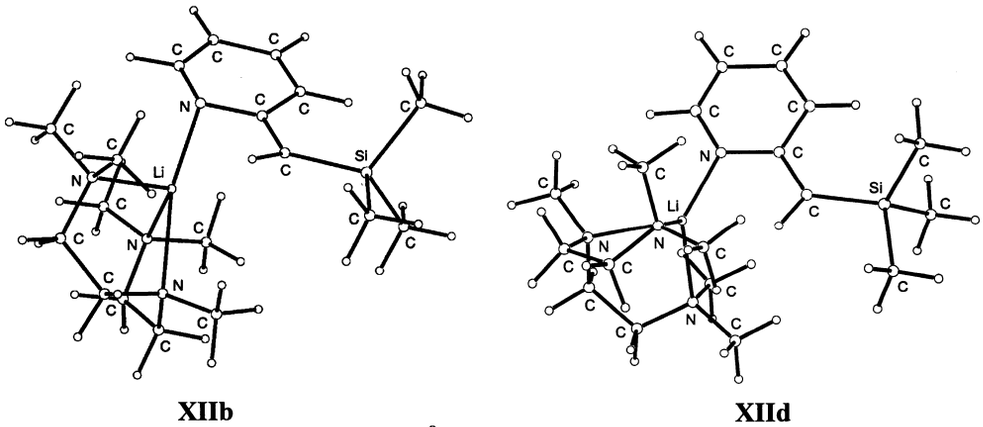

XIIb **XIId**

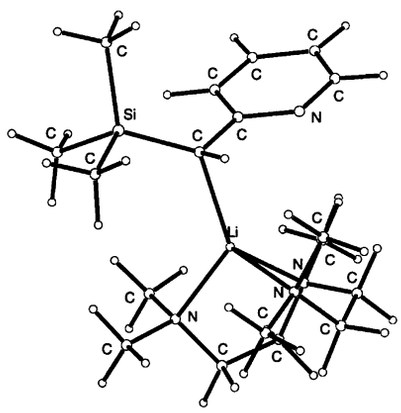

XIIe

Fig. 12 Optimised geometries of [**r**Li·pmdta] (**XIIb,d,e**).

span 2.250, 2.384, and 2.184 Å. **XIIe**, which is 5.7 kcal mol^{-1} less stable than **XIId**, contains a C–Li bond of length 2.193 Å and three Li–N bonds to pmdta. The pyridinium N is found 3.26 Å away from the Li.

Further inspection of models **XIIb** and **XIId** reveal that the main difference between them is orientation of the pmdta molecule within the complex. In **XIId** the open face of the (u-shaped) pmdta is pointing towards the C^7H–$SiMe_3$ portion of the **r** moiety, while in **XIIb** the closed face of the pmdta is pointing towards this portion. In the latter the Li·pmdta portion has slipped below the plane of the pyridine to minimise steric repulsion. Rotation of the pmdta portion by 180° in **XIId** and geometry re-optimisation, results in an identical geometry to that of **XIIb** and a similar exercise for **XIIb** results in the structure of **XIId**. The calculated energy difference between **XIIb** and **XIId** is too small to confidently state which is the more likely structure. However, their aforementioned calculated bond lengths are in reasonable agreement with those reported in Table 6 for complex **4**.

The situation for the **XIII** series is slightly different. As the sodium ion is much bigger than lithium, it is able to coordinate to more anionic sites and this is seen in this series. Thus in model **XIIId** the Na moves on optimisation to bond to the atoms of the aza-allyl portion and a similar movement occurs for model **XIIIe** to give an identical structure. The more stable structure of the **XIII** series by a mere 0.5 kcal mol^{-1} is **XIIIb** and this differs from the previous structure only in the orientation of the pmdta molecule. In **XIIIb** the open face of the pmdta is pointing away from the C^7H–$SiMe_3$ group, while in **XIIId** it is directed at this portion. The structure of **XIIIb** has Na lying below an extended plane of the pyridine ring and bonding to N (2.401 Å) and to C^7 (2.601 Å). The geometrical parameters of the N–C^2–C^7 portion (N–C^2 1.364, C^2–C^7 1.410 Å) indicate that the π electron conjugation has been reduced due to weak coordination of C^7 to Na. The distance between Na and the H attached to C^7 is calculated to be 2.44 Å. The pmdta bonds to the Na *via* three N–Na bonds of length 2.492, 2.534 and 2.572 Å. The energy of complexing of **r**Na with pmdta is found to be −27.6 kcal mol^{-1}. This series of calculations has shown that Na can effectively cope with more than four coordinating bonds and it is not surprising that the **r**Na·pmdta complex can dimerise while the corresponding Li complex remains monomeric.

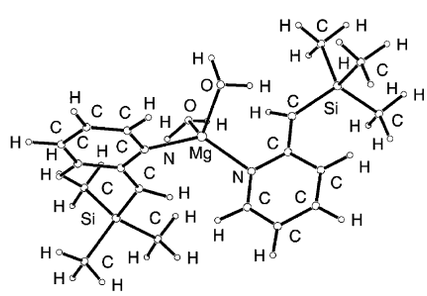

XIV

Fig. 13 Optimised geometry of [$(\mathbf{r})_2$Mg·$(H_2O)_2$] (**XIV**).

The next series of calculations (**XIV**), Fig. 13, examined the effect of donor solvents on the structure of $(\mathbf{r})_2$Mg. Water was chosen as a simple model to represent an oxygen-donating solvent such as hmpa and two water molecules were added to model **VIIb** so that initially the Mg was six coordinated. After geometry optimisation it was found that the Mg was only four coordinated; two bonds to O (2.047, 2.049 Å) and two bonds to N (2.055 Å). These values show reasonable agreement with the experimental distances reported herein. The C^7 atoms are stationed 3.1 Å away from the Mg and their orbitals revert to π conjugation with the N–C^2 unit giving bond lengths similar to those found in **r** (**II**) *i.e.* C^7–C^2 1.404 and C^2–N 1.369 Å. The calculated distance between Mg and the H bonded to

Table 8 Crystallographic details for complexes **1**–**5**

Compound	**1** [a]	**2** [b]	**3** [c]	**4** [d]	**5** [e]
Formula	$C_{36}H_{74}N_8Na_2Si_2$	$C_{36}H_{74}N_8K_2Si_2$	$C_{30}H_{60}N_6Na_2Si_2$	$C_{22}H_{46}N_4LiSi$	$C_{30}H_{64}N_8MgSi_2O_2P_2$
M_w	721.2	753.4	607.0	429.74	711.3
Specimen/mm	1.0 × 0.6 × 0.32	0.38 × 0.2 × 0.35	0.4 × 0.25 × 0.18	0.15 × 0.18 × 0.2	0.1 × 0.65 × 0.45
Crystal system	Monoclinic	Monoclinic	Orthorhombic	Monoclinic	Monoclinic
Space group	$P2_1/c$	$P2_1/n$	$C222_1$	$P2_1/n$	$P2_1/c$
a/Å	10.221(5)	10.274(3)	13.67(1)	7.6805(2)	13.489(4)
b/Å	21.645(10)	19.45(1)	15.72(1)	16.0419(2)	19.258(5)
c/Å	11.430(2)	12.10(2)	18.50(1)	18.9022(2)	17.536(4)
α/°	—	—	—	—	—
β/°	115.10(3)	99.89(8)	—	100.5403(8)	108.74(2)
γ/°	—	—	—	—	—
V/Å^3	2290	2382	3975	2290	4314
Z	2	2	4	4	4
$2\theta_{max}$/°	50	45	46	60.1	50
D_{calc}/g cm^{-3}	1.04_6	1.05_0	1.01_4	1.24_7	1.09_5
μ/cm^{-1}	1.3	2.8	1.4	1.72	2.1
T/K	298	298	298	123	298
N_{ind}	4015	3289	1560	6575	7628
N_{obs}	2324	1077	642	3683	2075
R_w	0.047	0.038	0.052	0.079	0.057
R	0.049	0.048	0.054	0.066	0.053

[a] $|\Delta\rho_{max}| = 0.24(2)$ e Å^{-3}. (x, y, z, $U_{iso})_H$ refined throughout. [b] (x, y, z, $U_{iso})_H$ refined for H(21–26), constrained for the remainder. Although the cells are similar, the last two Na, K complexes are not isomorphous (see text and Fig. 6). [c] (x, y, z, $U_{iso})_H$ refined for H(21), constrained at estimates for the remainder. [d] All H placed in calculated positions (r = 0.95 Å). [e] $|\Delta\rho_{max}| = 0.2_1$ e Å^{-3}. (x, y, z, $U_{iso})_H$ constrained throughout. *Variata*. Methyl groups 2 of each Me_2N component about P(2) were resolved and modelled as disordered over two sets of sites, occupancies set at 0.5 after trial refinement; concomitant components of the associated nitrogen atoms were not resolved.

C^7 is 2.6 Å. The resulting energy of complexing is −19.4 kcal mol^{-1}.

These calculations indicate that the preferred bonding mode between the metallic cation and **r** in the species **r**Li, **r**Na and (**r**)$_2$Mg involves interaction of the metal with the atoms of the aza-allyl species and a simultaneous lowering of the π-electronic conjugation in the aza-allyl region. In the presence of donor solvents that form strong coordinating bonds with the metallic cations, the interaction of the metal with the aza-allyl unit weakens and this is particularly true of the carbon atoms within this unit. Thus, for **r**Li·pmdta and (**r**)$_2$Mg·(H$_2$O)$_2$ the bonding between the metallic cation and **r** involves M–N bonds only. The aza-allyl unit benefits from the diminishing interaction with the metallic cation and increased π-electronic conjugation results. For **r**Li and **r**Na the preferred position of the C^7–SiMe$_3$ bond about the C^2–C^7 partial double bond is *cis* to the C^2–N bond. On addition of bulky solvent molecules to the metallic cation the favoured location is *trans* to the C^2–N bond. A consequence of this preference is that the hydrogen attached to C^7 is now adjacent to the metallic cation.

Conclusions

This structural and computational study on five alkali metal and magnesium complexes of Me$_3$Si substituted picolyl anions, [**r**Na·(pmdta)]$_2$, **1**, [**r**K·(pmdta)]$_2$, **2**, [**r**Na·(tmeda)]$_2$, **3**, [**r**′Li·(pmdta)], **4**, [(**r**)$_2$Mg·(hmpa)$_2$], **5**, reveals that, in the solid state at least, they will preferentially adopt an enamide rather than carbanion or aza-allyl configuration in the presence of one or more bulky coordinating Lewis base ligands. Steric and electronic effects influence the orientation of the Me$_3$Si groups relative to the N–M bond and give rise to close agostic M···C–H bonds in the solid state structures.

Experimental

All compound manipulations were carried out under strict inert atmosphere and dry conditions using a vacuum/argon line, Schlenk techniques and a high purity argon gas recirculating dry box. Prior to use, solvents were dried by reflux over Na–K alloy and stored over 4 Å molecular sieves. [(2-Pyr)(SiMe$_3$)CH$_2$, **r**H, and 6-Me-(2-Pyr)(SiMe$_3$)CH$_2$, **r**′H, were prepared according to the literature procedure.[2] ^{n}BuLi was purchased from Merck-Schuchardt and ^{n,s}Bu$_2$Mg from Aldrich. ^{n}BuNa and ^{n}BuK were prepared from the metathesis reaction of ^{n}BuLi and ^{t}BuOM (M = Na, K) in hexane and stored as solids. (Note: these solids are extremely pyrophoric). The ligands pmdta, tmeda and hmpa were refluxed over CaH$_2$, distilled and stored over 4 Å molecular sieves. NMR spectra were obtained on a Bruker AM-200 spectrometer with chemical shifts referenced to the C$_6$D$_6$ solvent. Elemental analyses were carried out by CMAS, Australia.

X-Ray crystallographic studies

X-Ray crystallography on complex **4** was carried out on an Enraf-Nonius, Kappa CCD (crystal mounted under oil), and for complexes **1**–**3** and **5** on a CAD 4 diffractometer (crystals mounted in capillaries, monochromatic Mo-Kα radiation, $\lambda = 0.7107_3$ Å; *T ca.* 295 K) to the specified level of redundancy, yielding N unique reflections, N_o with $I > n\sigma(I)$ (n = 3 for **1**, **2**, **3**; n = 2 for **5**) being considered 'observed' and used in the full matrix least squares refinement (non-hydrogen thermal parameter forms anisotropic; (x, y, z, $U_{iso})_H$ treatment as specified) after Gaussian absorption correction. Conventional residuals at convergence on $|F|$, R, R_w (statistical weights, derivative of $\sigma^2(I) = \sigma^2(I_{diff}) + 0.0004\sigma^2(I_{diff})$) are quoted. Neutral atom complex scattering factors were employed within the Xtal 3.4 program system.[19] Pertinent results are quoted below (noting individual diversities in procedure) and in the Figures and Tables.

See Table 8 for the crystallographic details for complexes **1**–**5**.

CCDC reference numbers 154200–154204.

See http://www.rsc.org/suppdata/dt/b0/b009596f/ for crystallographic data in CIF or other electronic format.

Syntheses

Complex 1, [rNa·(pmdta)]$_2$. **r**H (10 mmol, 1.67 g) was added dropwise to a chilled (0 °C) suspension of ^{n}BuNa (10 mmol, 0.80 g) in hexane (*ca.* 15 ml). The suspension immediately became dark yellow in colour, and was stirred for a further 1 h. pmdta (10 mmol, 2.08 ml) was added dropwise resulting in a

dark orange suspension. Hexane was removed *in vacuo*, replaced with toluene (*ca*. 10 ml) and warmed. Dissolution gave a dark orange solution. Orange crystals of **1** were obtained on cooling to 4 °C overnight. Yield 78%. mp 120–122 °C (black melt). Elemental analysis; Found (calc. for $C_{36}H_{74}N_8Na_2Si_2$); C 59.9 (60.0), H 10.7 (10.3), N, 15.8 (15.5)%.

Complex 2, [rK·(pmdta)]$_2$. **r**H (10 mmol, 1.67 g) was added dropwise to a chilled (0 °C) suspension of ^{n}BuK (10 mmol, 0.96 g) in hexane (*ca*. 15 ml). The suspension immediately became dark yellow in colour, and was stirred for a further 1 h. pmdta (10 mmol, 2.08 ml) was added dropwise resulting in a dark red suspension. Hexane was removed *in vacuo*, replaced with toluene (*ca*. 15 ml) and warmed. Dissolution gave a dark red solution. Orange crystals of **2** were obtained on cooling to 4 °C overnight. Yield 64%. mp 124–126 °C (black melt). Elemental analysis; Found (Calc. for $C_{36}H_{74}N_8NK_2Si_2$); C 57.0 (57.4), H 10.4 (10.0), N, 15.3 (14.9)%.

Complex 3, [rNa·(tmeda)]$_2$. **r**H (10 mmol, 1.67 g) was added dropwise to a chilled (0 °C) suspension of ^{n}BuNa (10 mmol, 0.80 g) in hexane (*ca*. 15 ml). The suspension immediately became dark yellow in colour, and was stirred for a further 1 h. tmeda (10 mmol, 1.51 ml) was added dropwise resulting in a dark orange suspension. Hexane was removed *in vacuo*, replaced with toluene (*ca*. 10 ml) and warmed. Dissolution gave a dark orange solution. Orange crystals of **3** were obtained on cooling to 4 °C overnight. Yield 73%. mp 164–166 °C. Elemental analysis; Found (Calc. for $C_{30}H_{60}N_6Na_2Si_2$); C 59.7 (59.3), H 10.6 (9.9), N 13.5 (13.8)%.

Complex 4, [r′Li·(pmdta)]$_2$. ^{n}BuLi (10 mmol, 1.6 M, 6.25 ml) in hexane was added dropwise to a chilled (−78 °C) solution of **r**′H (10 mmol, 1.81 g) in hexane (*ca*. 15 ml). The solution immediately became orange in colour, and was stirred for a further 1 h and allowed to warm to room temperature. pmdta (10 mmol, 2.08 ml) was added dropwise resulting in a dark orange suspension. Dissolution occurred on warming and gave a dark orange solution. Orange crystals of **4** were obtained on cooling to 4 °C overnight. Yield 65%. mp 129–132 °C. Elemental analysis; Found (Calc. for $C_{22}H_{46}N_4LiSi_2$); C 64.0 (63.6), H 10.3 (10.9), N 15.8 (15.6)%.

Complex 5, [(r)$_2$Mg·(hmpa)]$_2$. ^{n,s}Bu$_2$Mg (10 mmol, 1.0 M, 10 ml) in heptane was added dropwise to a chilled (−78 °C) solution of **r**H (10 mmol, 1.67 g) in hexane (*ca*. 15 ml). A colourless precipitate formed immediately. This was stirred for a further 1 h and allowed to warm to room temperature. hmpa (20 mmol, 3.48 ml) was added dropwise. Dissolution occurred on warming and gave a colourless to pale yellow solution. Colourless crystals of **5** were obtained on cooling to 4 °C overnight. Yield 76%. mp 156–157 °C. Elemental analysis; Found (Calc. for $C_{30}H_{64}N_8MgSi_2O_2P_2$); C 51.0 (50.6), H 9.3 (9.0), N 15.5 (15.7)%.

Acknowledgements

We thank the Australian Research Council and Monash University (P. C. A., C. L. R., B. A. R.) for financial support.

References

1 Review: T. van den Anker and C. L Raston, *J. Organomet. Chem.*, 1995, **200**, 289.
2 R. C. Papasergio, C. L. Raston, B. W. Skelton, P. Twiss and A. H. White, *J. Chem. Soc.*, *Dalton Trans.*, 1990, 1161; C. Jones, C. H. L. Kennard, C. L. Raston and G. Smith, *J. Organomet. Chem.*, 1990, **396**, C39.
3 C. J. Cardin, D. J. Cardin, S. P. Constantine, M. G. B. Drew, H. Rashid, M. A. Convery and D. Fenske, *J. Chem. Soc.*, *Dalton Trans.*, 1998, 2749; C. J. Cardin, D. J. Cardin, S. P. Constantine, A. K. Todd, S. J. Teat and S. Coles, *Organometallics*, 1998, **17**, 2144; G. Ossig, A. Meller, S. Freitag, R. Herbst-Irmer and G. M. Sheldrick, *Chem. Ber*, 1998, **126**, 2247; G. Ossig, A. Meller, C. Bronneke, O. Muller, M. Schafer and R. Herbst-Irmer, *Organometallics*, 1997, **16**, 2116; M. Hursthouse, K. J. Izod, M. Motavelli and P. Thornton, *Polyhedron*, 1996, **15**, 135; H. K. Lee, B.-S. Luo, T. C. W. Mak and W.-P. Leung, *J. Organomet. Chem.*, 1995, **489**, C71.
4 U. Pieper and D. Stalke, *Organometallics*, 1993, **12**, 1201.
5 W.-P. Leung, L.-H. Weng, R.-U. Wang and T. C. W. Mak, *Organometallics*, 1995, **14**, 4832.
6 L. D. Field, M. G. Gardiner, C. H. L. Kennard, B. A. Messerle and C. L. Raston, *Organometallics*, 1991, **10**, 3167.
7 P. C. Andrews, N. D. R. Barnett, R. E. Mulvey, W. Clegg, P. A. O'Neil, D. Barr, L. Cowton, A. J. Dawson and B. J. Wakefield, *J. Organomet. Chem.*, 1996, **518**, 85.
8 K. Gregory, M. Bremer, W. Bauer and P. v. R. Schleyer, *Organometallics*, 1990, **9**, 1485.
9 W. Clegg, S. Kleditzsch, R. E. Mulvey and P. O'Shaughnessy, *J. Organomet. Chem.*, 1998, **558**, 193.
10 F. Bosold, M. Marsch, K. Harms and G. Boche, *Z. Kristallogr.*, 1998, **213**, 619; T. Siefert, W. Storch and M. Vosteen, *Eur. J. Inorg. Chem.*, 1998, 1343; K. W. Henderson, A. E. Dorigo, Q.-L. Liu and P. J. Williard, *J. Am. Chem. Soc.*, 1997, **119**, 11855; J. Barker, D. Barr, N. D. R. Barnett, W. Clegg, I. Cragg-Hind, M. G. Davidson, R. P. Davies, S. M. Hodgson, J. A. K. Howard, M. Kilner, C. W. Lehman, I. Lopez-Solera, R. E. Mulvey, P. R. Raithby and R. Snaith, *J. Chem. Soc.*, *Dalton. Trans.*, 1997, 951; P. C. Andrews, G. A. Koutsantonis and C. L. Raston, *J. Chem. Soc.*, *Dalton Trans.*, 1995, 4059; I. Cragg-Hind, M. G. Davidson, F. S. Mair, P. R. Raithby and R. Snaith, *J. Chem. Soc.*, *Dalton Trans.*, 1993, 2423; D. Barr, W. Clegg, R. E. Mulvey, R. Snaith and D. S. Wright, *J. Chem. Soc*., *Chem. Commun.*, 1987, 716.
11 D. R. Armstrong, D. Barr, W. Clegg, R. E. Mulvey, D. Reed, R. Snaith and K. Wade, *J. Chem. Soc.*, *Chem. Commun.*, 1986, 869.
12 D. R. Armstrong, D. Barr, W. Clegg, S. M. Hodgson, R. E. Mulvey, D. Reed, R. Snaith and D. S. Wright, *J. Am. Chem. Soc.*, 1989, **111**, 4719.
13 D. Barr, W. Clegg, R. E. Mulvey and R. Snaith, *J. Chem. Soc.*, *Chem. Commun.*, 1984, 287.
14 R. I. Papasergio, C. L. Raston and A. H. White, *J. Chem. Soc.*, *Dalton Trans.*, 1987, 3085; S. I. Bailey, D. Colgan, L. M. Engelhardt, W.-P. Leung, R. I. Papasergio, C. L. Raston and A. H. White, *J. Chem. Soc.*, *Dalton Trans.*, 1986, 603.
15 W. Clegg, F. J. Craig, K. W. Henderson, A. R. Kennedy, R. E. Mulvey, P. A. O'Neil, D. Reed and D. Reed, *Inorg. Chem.*, 1997, **36**, 6238.
16 M. M. Olmstead, W. J. Gigsby, D. R. Chacon, T. Hascall and P. P. Power, *Inorg. Chim. Acta.*, 1996, **251**, 273.
17 Gaussian 94 (Revision A.1), M. J. Frisch, G. W. Trucks, H. B. Schlegel, P. M. W. Gill, B. G. Johnson, M. A. Robb, J. R. Cheeseman, T. A. Keith, G. A. Peterson, J. A. Montgomery, K. Raghavachari, M. A. Al-Laham, V. G. Zakrzewski, J. V. Ortiz, J. B. Foresman, J. Cioslowski, B. B. Stefanov, A. Nanayakkara, M. Challacombe, C. Y. Peng, P. Y. Ayala, W. Chen, M. W. Wong, J. L. Andres, E. S. Replogle, R. Gomperts, R. L. Martin, D. J. Fox, J. S. Binkley, D. J. Defrees, J. Baker, J. P. Stewart, M. Head-Gordon, C. Gonzalez and J. A. Pople, Gaussian Inc., Pittsburgh, PA, 1995.
18 W. J. Hehre, R. Ditchfield and J. A. Pople, *J. Chem. Phys.*, 1972, **56**, 2257; P. C. Hariharan and J. A. Pople, *Theor. Chim. Acta*, 1973, **28**, 213; J. D. Dill and J. A. Pople, *J. Chem. Phys.*, 1975, **62**, 2921.
19 S. R. Hall, G. S. D. King and J. M. Stewart (eds.), *The Xtal 3.4 User's Manual*, University of Western Australia, Lamb, Perth, 1995.